Article

Preparation of Fluorescent Magnetic Nanodiamonds and Cellular Imaging

In Pin Chang, Kuo Chu Hwang, and Chi-Shiun Chiang

J. Am. Chem. Soc., **2008**, 130 (46), 15476-15481 • DOI: 10.1021/ja804253y • Publication Date (Web): 22 October 2008

More About This Article

Additional resources and features associated with this article are available within the HTML version:

- Supporting Information
- Access to high resolution figures
- Links to articles and content related to this article
- Copyright permission to reproduce figures and/or text from this article

View the Full Text HTML

J|A|C|S
ARTICLES

Published on Web 10/22/2008

Preparation of Fluorescent Magnetic Nanodiamonds and Cellular Imaging

In Pin Chang,[†] Kuo Chu Hwang,*[,†] and Chi-Shiun Chiang[‡]

Departments of Chemistry and Biomedical Engineering and Environmental Sciences, National Tsing Hua University, Hsinchu, Taiwan

Received June 13, 2008; E-mail: kchwang@mx.nthu.edu.tw

Abstract: Magnetic nanodiamonds were prepared via solid-state microwave arcing of a nanodiamond−ferrocene mixed powder in a focused microwave oven. High-resolution transmission electron microscope (HRTEM) images show that a magnetic nanodiamond is composed of iron nanoparticles encapsulated by graphene layers on the surface of nanodiamonds. Fluorescence property was introduced onto magnetic nanodiamonds by chemical modification of magnetic nanodiamonds via surface grafting of poly(acrylic acids) and fluorescein *o*-methacrylate. Fluorescent magnetic nanodiamonds are water soluble with a solubility of ∼2.1 g/L. Cellular-imaging experiments show that fluorescent magnetic nanodiamonds could be ingested by HeLa cells readily in the absence of agonist (i.e., folate) moieties on the surface of nanodiamonds.

Introduction

Nanodiamonds (ND) obtained from detonation of explosives[1] are neither magnetic nor fluorescent. Because of their chemical stability, good biocompatibility, great thermal conductivity, and nontoxicity, ND are being developed as an alternative carrier for the transport of biologically active species into various cells, like many other nanomaterials including carbon nanotubes, quantum dots, gold nanoparticles, silica nanoparticles, etc.[2,3] Acid-reflux-treated ND were reported to conjugate with proteins,[4−6] cytochrome *c*,[7] lysozyme,[8] DNA,[9−12] antigen,[13] growth hormone,[14] and neurotoxin[15] and shown to be nontoxic to a variety of cells.[16−19] An active ND hydrogel served as a drug carrier to deliver apoptosis-inducing drugs effectively into living cells.[20] ND were reported to become fluorescent via chemical attachment of single-strand DNA followed by non-covalent adsorption of fluorescently labeled cDNA.[21] Otherwise, ND having nitrogen impurities can be made to fluoresce with red light ($\lambda_{em} \approx 700$ nm) via irradiation with highly energetic beams of protons (3 MeV) or electrons (∼ 2 MeV) followed by thermal annealing at ∼800 °C to create nitrogen-vacancy (N-V) defects,[17,22] but this process is tedious and inefficient. The quantum yield of fluorescence from the N-V defects was reported to be nearly unity with the fluorescence lifetime of 11.6 ns at 295 K.[23] Recently, it was reported that fluorescent ND could be produced by He^+ ion (40 keV) bombardment with 2 orders of magnitude higher efficiency than those in the proton or electron bombardment processes.[24] Besides the fluorescence,

[†] Department of Chemistry.
[‡] Department of Biomedical Engineering and Environmental Sciences.

(1) Greiner, N. R.; Phillips, D. S.; Johnson, J. D.; Volk, F. *Nature* **1988**, *333*, 440–442.
(2) For reviews of biomedical applications and cytotoxicity of nanoparticles/nanotubes, please see. (a) Lewinski, N.; Colvin, V.; Drezek, R. *Small* **2008**, *4*, 26–49. (b) Yang, W.; Thordarson, P.; Gooding, J. J.; Ringer, S. P.; Braet, F. *Nanotechnology* **2007**, *18*, 412001.
(3) For reviews of biomedical applications of metal nanoparticles, please see: (a) Lee, J.-H.; Huh, Y.-M.; Jun, Y.-W.; Seol, J.-W.; Jang, J.-T.; Song, H.-T.; Kim, S.; Cho, E.-J.; Yoon, H.-G.; Suh, J.-S.; Cheon, J. *Nat. Med.* **2007**, *13*, 95–99.
(4) Kong, X. L.; Huang, C. L.; Hsu, C. M.; Chen, W. H.; Han, C. C.; Chang, H. C. *Anal. Chem.* **2005**, *77*, 259–265.
(5) Hartl, A.; Schmich, E.; Garrido, J. A.; Hernando, J.; Catharino, S. C. R.; Walter, S.; Feulner, P.; Kromka, A.; Steinmüller, D.; Stutzmann, M. *Nat. Mater.* **2004**, *3*, 726–742.
(6) Huang, H.; Pierstorff, E.; Osawa, E.; Ho, D. *ACS Nano* **2008**, *2*, 203–212.
(7) Huang, L.-C. L.; Chang, H.-C. *Langmuir* **2004**, *20*, 5879–5884.
(8) Chao, J. I.; Perevedentseva, E.; Chung, P. H.; Liu, K. K.; Cheng, C. Y.; Chang, C. C.; Cheng, C. L. *Biophys. J.* **2007**, *93*, 2199–2208.
(9) Yang, W.; Auciello, O.; Butler, J. E.; Cai, W.; Carlisle, J. A.; Dieter, G.; Gruen, M.; Knickerbocker, T.; Lasseter, T. L.; Russell, J. N., Jr.; Smith, L. M.; Hamers, R. J. *Nat. Mater.* **2002**, *1*, 253–257.
(10) Takahashi, K.; Tanga, M.; Takai, O.; Okamura, H. *Diamond Relat. Mater.* **2003**, *12*, 572–576.
(11) Ushizawa, K.; Sato, Y.; Mitsumori, T.; Machinami, T.; Ueda, T.; Ando, T. *Chem. Phys. Lett.* **2002**, *351*, 105–108.
(12) Krüger, A. *Angew. Chem., Int. Ed.* **2006**, *45*, 6426–642.
(13) Kossovsky, N.; Gelman, A.; Hnatyszyn, H. J.; Rajguru, S.; Garrell, R. L.; Torbati, S.; Freitas, S. S.; Chow, G. M. *Bioconjugate Chem.* **1995**, *6*, 507–511.
(14) Cheng, C. Y.; Perevedentseva, E.; Tu, J. S.; Chung, P. H.; Chenga, C. L.; Liu, K. K.; Chao, J. I.; Chen, P. H.; Chang, C. C. *Appl. Phys. Lett.* **2007**, *90*, 163903–163905.
(15) Liu, K. K.; Chen, M. F.; Chen, P. Y.; Lee, T. J. F.; Cheng, C. L.; Chang, C. C.; Ho, Y. P.; Chao, J. I. *Nanotechology* **2008**, *19*, 205102.
(16) Schrand, A. M.; Huang, H.; Carlson, C.; Schlager, J. J.; Osawa, E.; Hussan, S. M.; Dai, L. *J. Phys. Chem. B* **2007**, *111*, 2–7.
(17) (a) Gruber, A.; Drabenstedt, A.; Tietz, C.; Fleury, L.; Wrachtrup, J.; von Borczyskowski, C. *Science* **1997**, *276*, 2012–2014. (b) Yu, S. J.; Kang, M. W.; Chang, H. C.; Chen, K. M.; Yu, Y. C. *J. Am. Chem. Soc.* **2005**, *127*, 17604–17605.
(18) Fu, C. C.; Lee, H. Y.; Chen, K.; Lim, T. S.; Wu, H.-Y.; Lin, P.-K.; Wei, P.-K.; Tsao, P. H.; Chang, H. C.; Fann, W. *Proc. Natl. Acad. Sci. U.S.A* **2007**, *104*, 727–732.
(19) Liu, K. K.; Cheng, C. L.; Chang, C. C.; Chao, J. I. *Nanotechnology* **2007**, *18*, 325102.
(20) Huang, H.; Pierstorff, E.; Osawa, E.; Ho, D. *Nano Lett* **2007**, *7*, 3305–3314.
(21) Rezek, B.; Shin, D. C.; Nakamura, T.; Nebel, C. E. *J. Am. Chem. Soc.* **2006**, *128*, 3884–3885.
(22) Jelezko, F.; Wrachtrup, J. *Phys. Status Solidi A* **2006**, *203*, 3207–3225.
(23) Collins, A. T.; Thomaz, M. F.; Jorge, M. I.; B, *J. Phys. C: Solid State Phys.* **1983**, *16*, 21772181v.].

10.1021/ja804253y CCC: $40.75

it is useful to have other properties simultaneously, such as magnetism. Nanoparticles with magnetic properties can serve not only as contrast reagents for magnetic-resonance imaging (MRI) but also as MRI-reporting markers in the nondestructive investigation of the biodistribution of nanoparticles (and thus surface-attached therapeutic molecules) in animals or human beings;[25] in such circumstances the animal or human subjects would not be sacrificed for study of the biodistribution of nanoparticles in various organs or tissues. Previous attempts were made to prepare magnetic ND by thermal decomposition of metal-containing compounds in mineral oil in the presence of ND.[26] Although ND and metal nanoparticles were observed to form aggregates in the TEM image, there is no direct evidence to show the presence of chemical binding between ND and metal nanoparticles. Physical ^{15}N-ion implantation was reported also to produce ferromagnetic ND via creation of sp^2/sp^3 defects.[27] The saturation magnetization of ferromagnetic ND so created is ~11.5 emu/g for a radiation dose of 5×10^{14} cm^{-2}. Here we report a novel and facile process to prepare ND with dual functions, namely, magnetic and fluorescent, and demonstrate its application as a cellular fluorescent marker.

Experimental Section

Preparation of Magnetic ND. Magnetic ND (MND) were prepared via formation of composite nanoparticles between ND and iron nanoparticles. Commercial ND (Micron + MDA, Element Six) are generally purified via acid refluxing and thereby have carboxylic acid and hydroxyl groups attached at the surface. The commercial ND were first loaded into a silica tube from which air was evacuated by pumping; the bottleneck was sealed with a flame. The ND were then thermally annealed at 1200 °C for 1 h to remove surface-attached polar functional groups. To prepare MND, we ground homogeneously thermally annealed ND powders (50 mg), ferrocene (Aldrich, 100 mg), and silicon powder (from broken silicon wafer, sizes in the range $1 \times 1 \times 1$ to $2 \times 2 \times 2$ mm^3, an equal volume). The silicon powder is replaceable by copper or other metal wires (length 1−2 cm). The powder of ND, ferrocene, and silicon particles well mixed in a silica tube was then evacuated to remove dioxygen and refilled with dinitrogen or argon (1 atm). The silica tube was loaded into the chamber of a focused microwave oven (2.45 GHz, Discover system, CEM Corp.) for microwave irradiation. This oven was set to be automatically switched off when the sample temperature attained 300 °C. During microwave irradiation microwave-induced arcing or sparks occurred violently among silicon particles (or among metal wires), leading to decomposition of ferrocene and formation of iron-filled carbon nanoparticles.[28] After focused microwave irradiation the residual ferrocene was washed away from the carbon soot with toluene. The carbon soot−toluene solution was sonicated. Magnetic carbon soot was collected from the toluene solution by an external magnet and examined in a transmission-electron microscope (TEM) (200 keV, JEOL JEM-2100, HRTEM). The saturation magnetization of the magnetic carbon soot was measured with a superconducting quantum-interference device (SQUID, Quantum Design, model MPMS5), and the powder X-ray pattern was recorded at beam line BL-01C2 SWLS PXRD in the National Synchrotron Radiation Research Center of Taiwan.

Surface Modification of Magnetic ND. To introduce hydrophilicity and fluorescent properties to MND we modified the covalent surface of the magnetic carbon soot.[29] To an aqueous solution (7 mL) containing magnetic carbon soot (50 mg) was added liquid acrylic acid (AA, Aldrich, 1 mL) and benzoylperoxide (BPO, 0.25 mL, 0.4 M) followed by ultrasonication (20 min) to make the carbon soot become well dispersed. The solution was transferred immediately to a domestic microwave oven (2.45 GHz, 600 W) and exposed to microwave irradiation for 10 s. During microwave irradiation the solution temperature rose rapidly, causing decomposition of the BPO radical initiator and initiating polymerization. This addition of acrylic acid−BPO−microwave irradiation process was repeated twice. The third time an additional component, namely, fluorescein *o*-methacrylate (FM, 10 mg in 1 mL THF), was added, and the solution was sonicated and irradiated with microwaves under the same conditions. The fluorescent moiety, i.e., fluorescein *o*-methacrylate, was added to the ND-containing solution at a subsequent stage of surface grafting to avoid close contact with the graphene shells as photoexcited fluorescein might be electronically quenched by the graphene shells on the ND surface. Finally, the surface-functionalized MND were collected and separated from free unbound polymers on repeated washing with solvents THF and H_2O and centrifugation (at 8000−12000 rpm). The structure of the surface-bound moieties was characterized by FTIR (Bomem model DA-83 FTS) and the amount determined by thermogravimetric analysis (TGA, Seiko SSC 5000) with temperature increased at 10 °C/min.

Cell Culture. HeLa cells (12.5×10^3 cells per well in 6-well plates) cultured in DMEM (Dulbecco's modified-eagle medium) supplemented with FBS (Fetal Bovine Serum, 10%) and penicillin−streptomycin (1%) were treated with PFM-PAA-grafted Fe@CNP-ND (0.1 mL, 47.62 μg /mL) for 24 h. The cells were washed with a phosphate buffer solution (PBS, pH 7.4), further fixed onto a glass slide using paraformaldehyde solution (4%) in PBS for 5 min, and washed with PBST (5% Tween-20 in PBS) solution three times; then Triton X-100 solution (1 mL) was added. After exposure to Triton X-100 (1 h), the HeLa cells were stained with DAPI (4′,6-diamidino-2-phenylindole, 1 ng/mL PBS, 30 min). The samples were examined under a confocal laser-scanning microscope (OLYMPUS FV500) equipped with an InGaN semiconductor laser (405 nm), an Ar laser (488 nm), and a He−Ne laser (543 nm).

Cytotoxicity. One milliliter of HeLa cell-containing solution (~2.12×10^3 cells/mL) was added to each well of a 24-well plate and incubated 1 day to allow cells to stick on the surface of the plate. Aliquots of a PBS buffer solution containing different amounts of ND or FMND were added to the 24-well plate, and the cell solutions were incubated for another 3 days. A 50 μL amount of a MTT aqueous solution (0.5 mg/mL) was added to each well of the 24-well plate 4 h before termination of the 3-days incubation, and the cells were allowed to incubate for another 4 h. Then, the upper layer of the solutions in the 24-well plate was discarded, and 1 mL of DMSO was added to each well to lyse cell membrane followed by pipet stirring. The final solution in each well was centrifuged at 13 000 rpm to remove any solid residues before measurements of the optical absorbance at 570 nm. The optical absorbances were converted to cell viabilities based on a standard curve (absorbance vs cell numbers) obtained from controlled experiments carried out

(24) Chang, Y.-R.; Lee, H.-Y.; Chen, K.; Chang, C.-C.; Tsai, D.-S.; Fu, C.-C.; Lim, T.-S.; Tzeng, Y.-K.; Fang, C.-Y.; Han, C.-C.; Chang, H.-C.; Fann, W. *Nat. Nanotechnol.* **2008**, *3*, 284–288.
(25) Lu, C.-W.; Hung, Y.; Hsiao, J.-K.; Yao, M.; Chung, T.-H.; Lin, Y.-S.; Wu, S.-H.; Hsu, S.-C.; Liu, H.-M.; Mou, C.-Y.; Yang, C.-S.; Huang, D.-M.; Chen, Y.-C. *Nano Lett.* **2007**, *7*, 149–154.
(26) Gubin, S. P.; Popkov, O. V.; Yurkov, G. Y.; Nikiforov, V. N.; Koksharov, Y. A.; Eremenko, N. K. *Diamond Relat. Mater.* **2007**, *16*, 1924–1928.
(27) Talapatra, S.; Ganesan, P. G.; Kim, T.; Vajtai, R.; Huang, M.; Shima, M.; Ramanath, G.; Srivastava, D.; Deevi, S. C.; Ajayan, P. M. *Phys. Rev. Lett.* **2005**, *95*, 097201.
(28) Liang, Y. C.; Hwang, K. C.; Lo, S. C. *Small* **2008**, *4*, 405–409.
(29) Hsin, Y. L.; Lai, J. Y.; Hwang, K. C.; Lo, S. C.; Chen, F. R.; Kai, J. J. *Carbon* **2006**, *44*, 3328–3335.

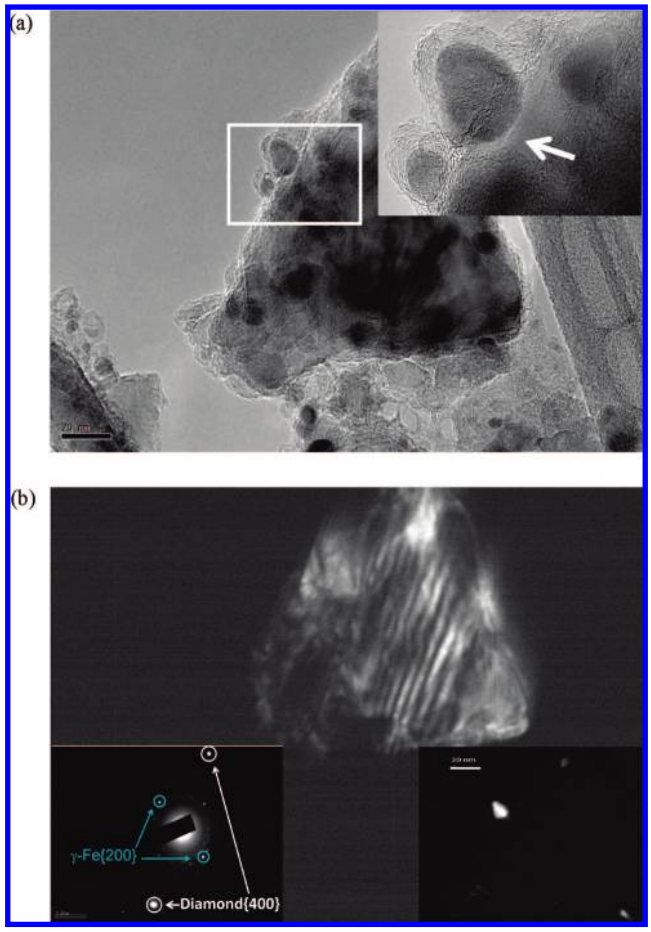

Figure 1. (a) Bright-field TEM image of Fe@CNP-ND produced from microwave arcing. (Inset) High- resolution TEM image of Fe@CNP-ND. The location indicated with a white arrow is absent from graphene layers. (b) Dark-field TEM image of the ND{400} plane. Bottom left inset in (b) is the electron diffraction pattern from the ND in (a). Bottom right inset in (b) is the dark-field TEM image of the γFe {200} plane.

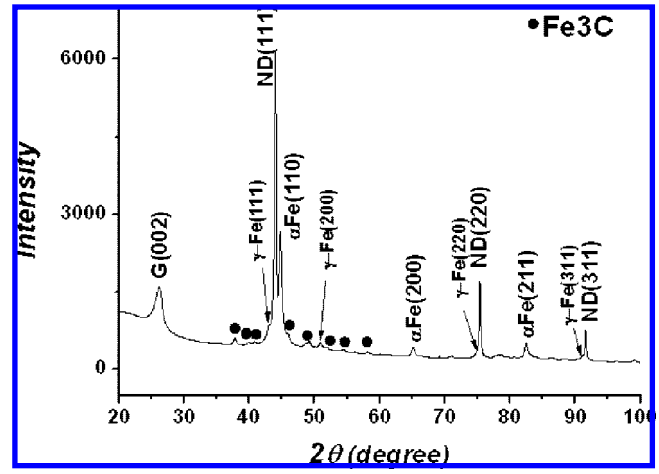

Figure 2. Powder X-ray diffraction (PXRD) pattern of Fe@CNP-ND. These data were obtained at beam line BL-01C2 SWLS PXRD in the National Synchrotron Radiation Research Center, Taiwan.

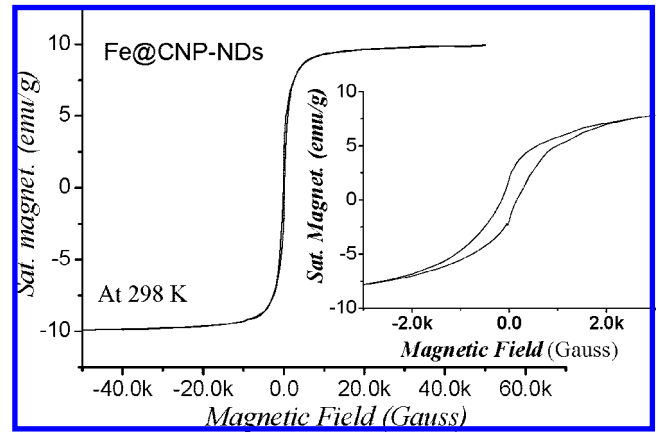

Figure 3. Saturation magnetization of Fe@CNP-ND as a function of external magnetic field at 298 K. (Inset) Hysteresis loop of saturation magnetization of the Fe@CNP-ND sample.

under the same condition except that no ND or FMND were added during cell culture processes.

Results and Discussion

Magnetic ND. Magnetic ND (MND) were produced via a novel microwave-arcing process[28,30] using ND powders and ferrocene as precursors in the presence of silicon powder. Upon microwave irradiation in a focused microwave oven electric arcing occurred among the silicon particles, which decomposed the ferrocene molecules and formed iron nanoparticles and graphene sheets.[28,30] These iron nanoparticles and ND were bound together with graphene sheets to form a new composite nanomaterial. Figure 1a shows a few graphene layers on the surface of ND. Many iron nanoparticles (size 5−20 nm) were wrapped inside graphene layers on the surface of large ND. The proportion of free core−shell iron−carbon nanoparticles (Fe@CNP) is limited; nearly all ND were covered with iron nanoparticles and graphene layers. The magnified TEM image (inset in Figure 1a and also Figure S1, Suppporting Information) shows clearly that the graphene layers about the iron nanoparticles are not symmetric; there is no graphene layer at the interface between an iron nanoparticle and the ND (location indicated with a white arrow), indicating that iron nanoparticles were chemically fixed (by graphene layers) on the ND surface instead of being merely physically deposited. Electron-diffraction measurement of the ND in Figure 1a shows the presence of diffraction spots from the ND(400) crystalline face (large circles in the bottom left inset of Figure 1b) and γ-Fe {200}crystalline face. The bright-field image of ND contributing to the ND(400) diffraction spot is shown in Figure 1b, which was obtained by limiting the detector at the (400) diffraction spot. Figure 1b shows clearly that the TEM image in Figure 1a is indeed a crystalline ND instead of a large piece of amorphous carbon. The inset at the bottom right of Figure 1b shows the location of γ-Fe nanoparticles which contribute to the γ-Fe {200}diffraction signal in the bottom left inset of Figure 1b. Measurement by powder X-ray diffraction (PXRD) of the ND−carbon soot shows the presence of ND, α-Fe, γ-Fe, graphene layers, and residual Fe_3C (see Figure 2). The saturation magnetism of iron−carbon nanoparticle ND using a superconducting quantum interference device (SQUID, Quantum Design, model MPMS5) near 295 K is ∼10 emu/g and the coercivity ∼155 G (see Figure 3). The saturation magnetization is much smaller than the values 35 and 216 emu/g for quasi-pure Fe@CNP[28] and bulk iron,[31] respectively, due mostly to the weight dilution by the ND, but the coercivity is much larger

(30) Hsin, Y. L.; Lin, C. F.; Liang, Y. C.; Hwang, K. C.; Horng, J. C.; Ho, J. A.; Lin, C. C.; Hwu, R. J. R. *Adv. Funct. Mater.* **2008**, *18*, 1–9.

Scheme 1. Schematic Process for Surface Functionalization of Magnetic NDs

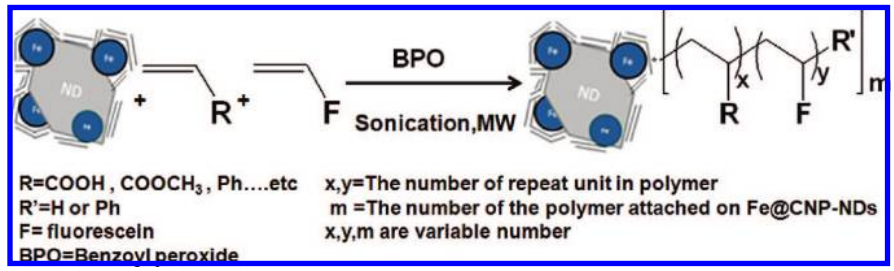

than 115 G for free Fe@CNP,[28] indicating that iron nanoparticles are less prone to switch magnetic subdomains than free Fe@CNP. The large coercivity is consistent with the TEM observation that most iron nanoparticles were chemically bound by graphene layers instead of being physically adsorbed on the surface of 'heavy' ND.

Fluorescent Magnetic ND (FMND). To introduce fluorescent properties we subjected magnetic ND to surface functionalization to attach covalently fluorescent moieties on the surface. As the C═C double bonds on surface graphene layers are chemically reactive toward free radicals, the MND can be surface grafted with almost any C═C double-bond-containing fluorescent monomer,[29] such as fluorescein *o*-methacrylate (see Scheme 1). During the radical-initiated polymerization the oligomeric radicals attack the C═C double bonds on the surface graphene layer of MND and form chemical bonds. After repeated washing and centrifugation MND were separated from free, unbound monomers and polymers. Figure 4 shows FTIR spectra of thermally annealed ND, MND as produced, PAA- and PFM-PAA-grafted Fe@CNP-ND. The weak C−H bond stretching band at ∼2980 cm^{-1} that exists in all samples is attributed to the terminal C−H bonds on the ND surface. The weak band at 1720 cm^{-1} and strong band at ∼1100 cm^{-1} in Figure 4a are attributed to residual C═O and C−O stretching modes, respectively. Thermal annealing of commercial ND at 1200 °C for 1 h apparently failed to completely remove oxygen atoms from the surface of ND. The moderately intense band at ∼1602 cm^{-1} originates from C═C double bonds of the surface graphene layers on ND. After solid-state microwave arcing to produce MND (see Figure 4b), the weak band at 1720 cm^{-1} associated with a C═O stretching mode disappears. Surface grafting of PAA onto MND is evident from the appearance of a carboxylic C═O stretching mode at 1725 cm^{-1} in addition to the broad absorption at 3400 cm^{-1} associated with the carboxylic O−H stretching mode (see Figure 4c). When FM (in a small proportion) was added to PAA in the surface functionalization, an additional weak band at ∼1765 cm^{-1} attributed to the stretching mode of the ester carbonyl (C═O) group of fluorescein moieties was observed (see Figure 4d). The amount of surface-functionalized moieties on Fe@CNP-ND was determined with thermogravimetric analysis (TGA). As shown in Figure 5 the onset of a rapid loss of mass at ∼500 °C (see top trace in Figure 5) is due to degradation of surface graphene layers of Fe@CNP-ND, consistent with the TGA pattern of Fe@CNP.[28] For a PFM- and PAA-grafted sample there is an additional loss of mass between 250 and 400 °C, which is due to the surface-grafted PFM and PAA oligomer side chains on the Fe@CNP-ND surface. The temperature of the onset of degradation of surface-grafted PAA side chains is the same as that reported for surface-grafted PAA on multiwalled carbon nanotubes.[29] Overall, the amount of surface-grafted PFM and PAA on the ND surface accounts for ∼22 wt % of the FMND. The surface-modified MND became redispersed in water satisfactorily without precipitation for several hours and were collected with an external magnet (see the inset in Figure 6). Upon UV irradiation the MND show bright, broadband, yellow-green fluorescence (see Figure 6 and the inset) with an emission maximum at 522 nm, which originates from the surface-grafted, photochemically excited fluorescein moieties. The color of the fluorescence can be tuned depending on the fluorescent monomers used in the surface functionalization process.

Cellular Imaging. To demonstrate the application of FMND as cellular fluorescence markers we incubated the FMND with HeLa cells. As shown in the confocal optical-microscopic

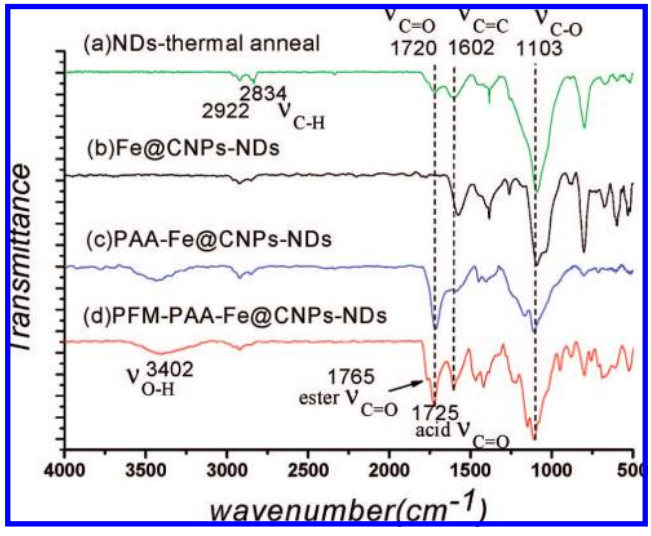

Figure 4. FTIR (Bomem model DA-83 FTS) spectra of (a) NDs, (b) Fe@CNP-NDs, (c) PAA-grafted Fe@CNP-NDs, and (d) PFM-PAA-grafted Fe@CNP-NDs. The assignments of stretching modes are as labeled in the figure.

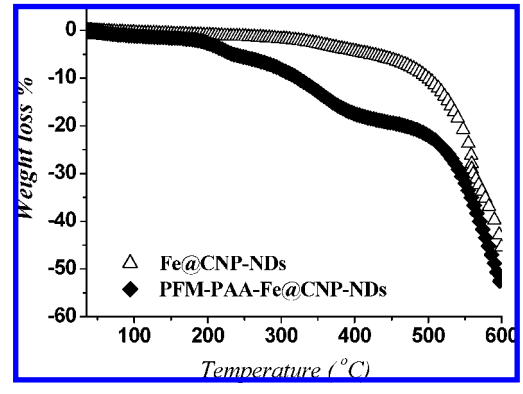

Figure 5. Thermogravimetric analysis of Fe@CNP-ND (Δ) as produced and PFM-PAA-grafted Fe@CNP-ND (◆) in the presence of air.

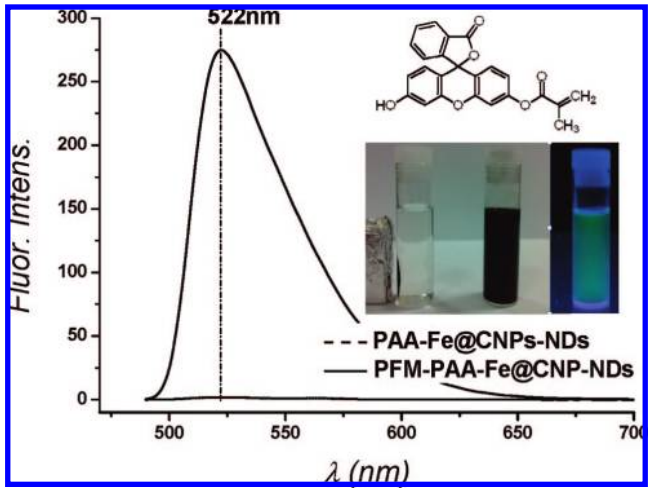

Figure 6. Fluorescence spectra (λ_{ex} = 475 nm) of PFM-PAA-grafted Fe@CNP-ND (solid line) and PAA-grafted Fe@CNP-ND (dashed line). The PAA-grafted Fe@CNP-ND were mixed physically with fluorescein *o*-methacrylate, washed with solvents, and filtered to remove physically absorbed fluorescein. (Inset) An aqueous solution of PFM-PAA-grafted Fe@CNP-ND (solubility ≈ 2.1 g/L) with (left) and without (middle) an external magnet. The yellow-green fluorescent image (right) of a PFM-PAA-grafted Fe@CNP-ND aqueous solution upon exposure to UV light.

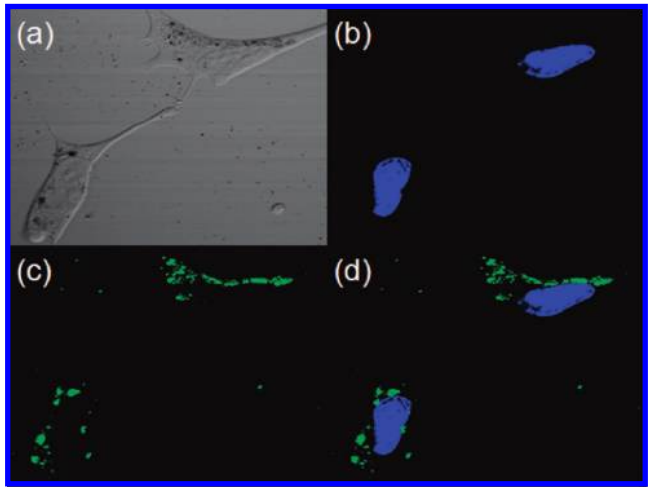

Figure 7. Vertical cross-sectional optical images of HeLa cells incubated with PFM-PAA-grafted Fe@CNP-ND for 24 h. The image of PFM-PAA-Fe@CNP-ND internalized into a HeLa cell under visible light (top left). The nuclei of HeLa cells were stained with DAPI dye (blue) (top right). The optical images of nucleus were recorded with a DAPI filter (λ_{ex}= 400−418 nm, λ_{em}= 450−465 nm). The green fluorescence in the bottom left image originates from PFM-PAA-grafted Fe@CNP-ND under a FITC filter (λ_{ex}= 478−495 nm, λ_{em}= 510−555 nm) (bottom left). The optical image shown in the bottom right is an overlapped image of the stained nucleus and the fluorescence of PFM-PAA-grafted Fe@CNP-ND (bottom right). The confocal optical image shows that PFM-PAA-grafted Fe@CNP-ND distribute around the nucleus (blue).

images (see Figure 7) the FMND were ingested well by HeLa cells. Figure 7 shows that most ingested FMND distributed in the cytoplasm regime without entering the nucleus (as labeled by a DAPI blue dye). To enter the nucleus regime generally requires a nuclear location signal (NLS, a short peptide, such as Pro-Lys-Lys-Lys-Arg-Lys-Val) moiety to assist binding to the nucleus membrane.[32] Carboxylic-acid-functionalized ND were reported to be internalized into the cytoplasm regime of macrophage RAW cells without entering the nucleus.[11] The FMND have no surface-bound folate moiety, an agonist moiety toward the folate receptors (FR) on the membrane surface of HeLa cells. Folate receptor is a glycosylphosphatidyl-inositol (GPI)-linked membrane glycoprotein with a molecular mass of about 38−40 kDa and a large affinity (K_D = 0.1 nM) toward folic-acid moieties. There are many folate receptors on the membrane surface of many tumor cells, such as ovarian, uterus, nasopharyngeal carcinoma, etc., but few on normal cells.[33] Having the folate moieties, nanoparticles can be internalized by HeLa cells via receptor-mediated endocytosis.[34] In the absence of folate moieties FMND can still be ingested by HeLa cells, indicating that there a nonreceptor-mediated endocytosis pathway exists in HeLa cells. Nonreceptor-mediated endocytosis seems to be a general process occurring in various cells upon ingestion of nanoparticles without having surface-grafted agonists, for example, an intake of carboxylic-acid-functionalized ND by 293T human kidney cells,[17] macrophage RAW cells,[20] human lung A549 epithelial cells and HFL-1 normal fibroblasts,[19] carbon dots by human breast-cancer MCF-7 cells,[35] silica-coated iron oxide nanoparticles by human mesenchymal stem cells (hMSC),[25] gold nanoparticles by C166 mouse endothelial cells,[36] etc. It has been shown that nonreceptor-mediated endocytosis occurs frequently in HeLa cells.[37] In the literature, it was recently reported that internalization of gold nanoparticles as well as the subsequent cell responses, including cell death and protein expression, are strongly dependent on the nanoparticle sizes.[38] It was also reported that gold nanoparticles could penetrate directly through the surface membrane of mammalian cells,[39,40] whereas in the case of cellular uptake of short SWNTs Pantarotto et al.[41] suggested a nonendocytotic mechanism via direct insertion and diffusion of SWNTs through cell membrane. Such a suggestion, however, was challenged by Dai and workers, who designed experiments to show that short SWNTs were internalized by cells via a clathrin-dependent endocytosis mechanism.[42] Exactly how ND enters and interacts with cell membranes is a complicated issue and will be investigated in the future.

Regarding the biocompatibility or cytotoxicity of FMND, MTT (3-[4,5-dimethylthiazol-2-yl]-2,5-diphenyltetrazolium bromide) experiments were carried using HeLa cells to examine the cell viability. As shown in Figure 8 the cell viabilities at various amounts of FMND are slightly lower than those of ND under the same conditions. Under the cellular imaging condition used in the confocal optical microscope experiments where the

(31) *CRC Handbook of Chemistry and Physics*, 72nd ed.; Lide, D. R., Ed.; Chemical Robber: Boca Raton, FL, 1991−1992; pp 12−95.
(32) Kalderon, D.; Roberts, B. L.; Richardson, W. D.; Smith, A. E. *Cell* **1984**, *39*, 499–509.
(33) Gabizon, A.; Horowitz, A. T.; Goren, D. *Bioconjugate Chem.* **1999**, *10*, 289–298.
(34) Zhang, Q. I.; Xiang, G.; Zhang, Y.; Yang, K.; Fan, W.; Lin, J.; Zeng, F.; Wu, J. *J. Pharm. Sci.* **2006**, *95*, 2266–2275.
(35) Cao, L.; Wang, X.; Mexziani, M. J.; Lu, F.; Wang, H.; Luo, P. G.; Lin, Y.; Harruff, B. A.; Veca, L. M.; Murray, D.; Xie, S.-Y.; Sun, Y.-P. *J. Am. Chem. Soc.* **2007**, *129*, 11318–11319.
(36) Rosi, N. L.; Giljohann, D. A.; Thaxton, C. S.; Lytton-Jean, A. K. R.; Han, M. S.; Mirkin, C. A. *Science* **2006**, *312*, 1027–1030.
(37) Olson, J. K.; Grose, C. *J. Virol.* **1997**, *71*, 4042–4052.
(38) Jiang, W.; Kim, B. S.; Rutka, J. T.; Chan, W. C. W. *Nat. Nanotechnol.* **2008**, *3*, 145–150.
(39) Verma, A.; Uzun, O.; Hu, Y.; Han, H.-S.; Watson, N.; Chen, S.; Irvine, D. J.; Stellacci, F. *Nat. Mater.* **2008**, *7*, 588–595.
(40) Xia, T.; Rome, L.; Nel, A. *Nat. Mater.* **2008**, *7*, 519–520.
(41) Pantarotto, D.; Briand, J.; Prato, M.; Bianco, A. *Chem. Commun.* **2004**, 16–17.
(42) Wong, N.; Kam, S.; Liu, Z.; Dai, H. J. *Angew. Chem., Int. Ed.* **2006**, *45*, 577–581.

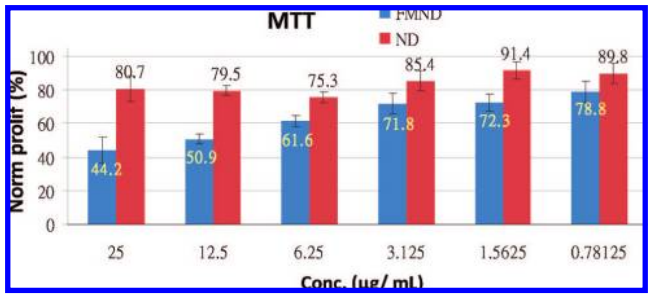

Figure 8. Cell viabilities of HeLa cells in the presence of various amounts of authentic ND and fluorescent magnetic ND.

concentration of FMND is 0.25 μg/mL the cell viabilities are higher than 79% and 90% for FMND and ND, respectively. Overall, the FMND can be considered to have low cytotoxicity toward HeLa cells.

Conclusion

We developed a facile process to prepare ND with dual fluorescent and magnetic properties. Magnetic ND were first prepared via a novel microwave-arcing process using pristine ND and ferrocene as precursors. Iron nanoparticles were chemically bound onto the surface of ND by graphene layers. The magnetic ND have a saturation magnetization of ~10 emu/g and a coercivity field 155 G. We showed that via covalent surface grafting of organic fluorescent molecules the MND become converted to fluorescent MND. The color of fluorescence is readily tunable depending on the polymerizable fluorescent monomer used in the surface grafting process. The FMND have an aqueous solubility of ~2.1 g/L and are collectible with an external magnet, which is important in many applications. A cellular-imaging experiment shows clearly that these water-soluble FMND can be ingested readily by HeLa cells, likely via a nonreceptor-mediated endocytosis, to enter and remain in the cytoplasm regime without entering the nucleus. Our work shows that water-soluble FMND have great potential in biomedical applications to serve as biocompatible cargos to transport various biologically active species, such as proteins, DNA, signal-transduction molecules, and drugs, into cells for various biomedical investigation or treatment of diseases.

Acknowledgment. The financial support from the National Science Council, Taiwan, is gratefully acknowledged. The authors are also thankful to Ms. Li lan Chiu for her cytotoxicity measurements.

Supporting Information Available: Additional high-resolution TEM images of Fe@CNP-ND produced from a solid-state microwave-arcing process are available. This material is available free of charge via the Internet at http://pubs.acs.org.

JA804253Y